RESEARCH ARTICLE | MAY 01 2023

# Sliding friction on ice

**Special Collection:** Adhesion and Friction

N. Miyashita ; A. E. Yakini; W. Pyckhout-Hintzen ; B. N. J. Persson



*J. Chem. Phys.* 158, 174702 (2023)
https://doi.org/10.1063/5.0147524

The Journal of Chemical Physics ARTICLE scitation.org/journal/jcp

# Sliding friction on ice

Cite as: J. Chem. Phys. 158, 174702 (2023); doi: 10.1063/5.0147524
Submitted: 23 February 2023 • Accepted: 13 April 2023 •
Published Online: 1 May 2023



N. Miyashita,[1] A. E. Yakini,[2,3] W. Pyckhout-Hintzen,[4] and B. N. J. Persson[2,3,a)]

## AFFILIATIONS

[1]The Yokohama Rubber Company, 2-1 Oiwake, Hiratsuka, Kanagawa 254-8601, Japan
[2]Peter Grünberg Institute (PGI-1), Forschungszentrum Jülich, 52425 Jülich, Germany
[3]MultiscaleConsulting, Wolfshovener Str. 2, 52428 Jülich, Germany
[4]Neutron Scattering and Biological Matter (JCNS-1/IBI-8), Forschungszentrum Jülich, 52425 Jülich, Germany

**Note:** This paper is part of the JCP Special Topic on Adhesion and Friction.
[a)]**Author to whom correspondence should be addressed:** b.persson@fz-juelich.de

## ABSTRACT

We study the friction when rectangular blocks made from rubber, polyethylene, and silica glass are sliding on ice surfaces at different temperatures ranging from −40 to 0 °C, and sliding speeds ranging from 3 $\mu$m/s to 1 cm s$^{-1}$. We consider a winter tire rubber compound both in the form of a compact block and as a foam with ~10% void volume. We find that both rubber compounds exhibit a similar friction on ice for all studied temperatures. As in a previous study at low temperatures and low sliding speeds, we propose that an important contribution to the friction force is due to slip between the ice surface and ice fragments attached to the rubber surface. At temperatures around 0 °C (or for high enough sliding speeds), a thin pre-melted water film will occur at the rubber–ice interface, and the contribution to the friction from shearing the area of real contact is small. In this case, the dominant contribution to the friction force is due to viscoelastic deformations of the rubber by the ice asperities. The sliding friction for polyethylene (PE) and silica glass (SG) blocks on ice differs strongly from that of rubber. The friction coefficient for PE is ~0.04 – 0.15 and is relatively weakly velocity dependent except close to the ice melting temperature where the friction coefficient increases toward low sliding speeds. Silica glass exhibits a similarly low friction as PE for $T > -10$ °C but very large friction coefficients (of order unity) at low temperatures. For both PE and SG, unless the ice track is very smooth, the friction force depends on the position $x$ along the sliding track. This is due to bumps on the ice surface, which are sheared off by the elastically stiff PE and SG blocks, resulting in a plowing-type of contribution to the friction force. This results in friction coefficients, which locally can be very large ~1, and visual inspection of the ice surface after the sliding acts show ice wear particles (white powder) in regions where ice bumps occur. Similar effects can be expected for rubber blocks below the rubber glass transition temperature, and the rubber is in the (elastically stiff) glassy state.





## I. INTRODUCTION

Friction on ice is a topic with a long history[1–10] starting with a study by Faraday[11] where he proposed that ice is covered by a liquid-like water layer.[12] Ice pre-melting, leading to a thin (nanometer) liquid-like water layer at the ice–vapor interface, has been observed in many experiments and computer simulations.[13–21] However, it is not clear whether such a layer of high mobility water molecules occurs at the interface between ice and another solid. Thus, the fact that ice frozen on most solid surfaces cannot be removed easily has been interpreted as an indication of the absence of a pre-melted water film. However, because of surface roughness, this conclusion may be incorrect (see Fig. 1).[22,23] Here, we note that ice in contact with solids with hydrophilic surfaces, such as most metal oxides, typically shows ~3 times higher adhesion and shear strength than for hydrophobic materials like many polymers.[24] This could be caused by air bubbles formed at the water–polymer interface before the water freezes.

An alternative explanation for the low friction on ice was proposed by Thomson. He suggested that the liquid-like layer is due to pressure melting.[25] Pressure melting was often used as an explanation for the low friction on ice, but in most cases, plastic flow of the ice will occur before the pressure is large enough to melt the ice.

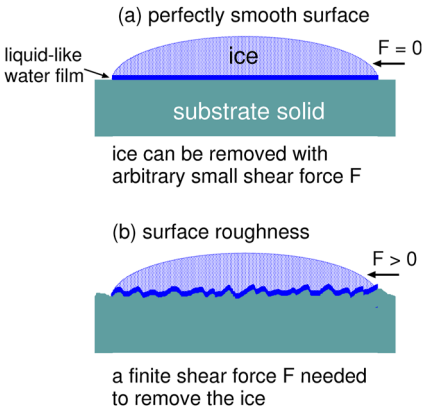


**FIG. 1.** Water droplet frozen on a substrate. (a) If the substrate is perfectly smooth, and if a thin pre-melted (liquid-like) water film would occur at the ice–countersurface interface, an arbitrary small shear force $F$ could displace the ice. (b) If the substrate has surface roughness, a finite shear force $F$ is needed to displace the ice. In case (b), the force $F$ could involve shearing the ice at the interface (cohesive failure) that would depend on the shear yield stress of the ice. We note that "perfect" silica glass surfaces prepared by cooling from the melted state (as for float glass) have frozen capillary waves with the fractal dimension $D_f = 3$ and while the rms roughness amplitude is very small (about $\approx 0.27$ nm), the rms slope is of order unity (see the Appendix). This roughness occurs mainly on length scales shorter than the wavelength of light and thus does not scatter light and cannot be observed optically. Theory shows that this roughness is enough to generate a cohesive failure when removing ice frozen onto the glass surface,[23] even when a pre-melted water film of a few monolayers occurs at the glass–ice interface, as expected close to the ice bulk melting temperature.[22] This explains why it is hard to remove ice from a car's windshield in winter, even when the temperature is close to the ice melting temperature.

At high enough sliding speed, frictional heating will result in melting of the ice surface. This was first suggested by Bowden and Hughes[26,27] and is now considered to be the main reason for the low friction of ice at high sliding speed.[26]

Whether a liquid-like pre-melted water film can form between ice and another solid depends on the chemical nature of the solid.[28] However, experimental results indicate that a liquid-like layer may occur below the bulk melting temperature even for ice in contact with ice if the two crystal lattices are incommensurately oriented (e.g., rotated). This is also consistent with the fact that many crystalline solids start to melt at grain boundaries before the whole material melts.[29,30] Still, the frictional shear properties of this liquid-like layer may be very different from that occurring at the interface between, e.g., Teflon and ice.[17]

In this paper, we study the friction for rubber, polyethylene, and silica glass blocks sliding on ice. Rubber friction on ice has many applications and is particularly important for understanding the grip of tires on icy road surfaces.[31–36] The friction between polyethylene and ice is importance for skiing where skis made from (high-density) polyethylene are often used.[37,38] Finally, the friction (or shear strength) between silica glass and ice is of interest in many applications where one needs to remove ice or frost from glass, e.g., from the windscreen of a car.

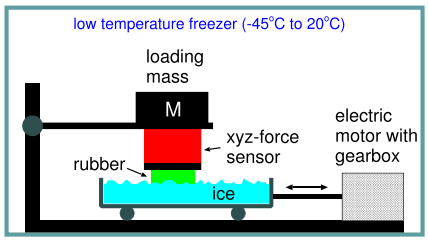


**FIG. 2.** Schematic picture of the low-temperature friction instrument allowing for linear reciprocal motion.

## II. EXPERIMENTAL

### A. Low temperature friction tester

We have performed ice friction measurements using our low temperature linear friction slider. In this set-up, the temperature can be changed from room temperature down to −40 °C. The rubber is glued on the sample holder (aluminum plate) (see Fig. 2), which is attached to the force cell. The rubber specimen can move with the carriage in the vertical direction to adapt to the substrate profile. The normal load can be changed by adding steel plates on top of the force cell. The substrate sample is attached to the machine table that is moved by a servo drive via a gearbox in a translational manner. We control the relative velocity between the rubber specimen and the substrate sample, while the force cell acquires information about normal force as well as the friction force.

To change the temperature, and to avoid (or reduce) the condensation of moisture in the atmosphere on the rubber and ice surfaces, the whole set-up is placed inside a deep-freezer. We slide the rubber sample over the ice surface with various velocities to gain information on the velocity and temperature dependency of the friction coefficient. With the current configuration, it is possible to vary the rubber specimen velocities between 1 $\mu$m/s and 12.5 mm s$^{-1}$. A heating system built into the set-up allows the raise of the temperature after the experiment is over.

### B. Ice surface

The ice surface was produced according to the procedure I1 described in Ref. 34. Thus, distilled water was poured into an aluminum box and frozen to make a thin ice layer. This process was repeated to obtain a thick ice substrate without (or with reduced) surface unevenness resulting from the freezing-induced expansion of water (note: ice assumes a larger volume than water at 0 °C). In Ref. 34, it was shown that the surface roughness power spectrum of the ice surface prepared in this way is very similar to the power spectra obtained from ice surfaces produced using other and different procedures. We did not study the surface topography of the ice surface used in the present study, but we will assume that it is similar to the ice surface I1 studied in Ref. 34.

The red line in Fig. 3 shows the surface roughness power spectrum of the ice surface used in the viscoelastic friction calculations, which is the same as used in Ref. 1. The green, blue, black and pink lines are the power spectra of the surfaces of rubber compounds A

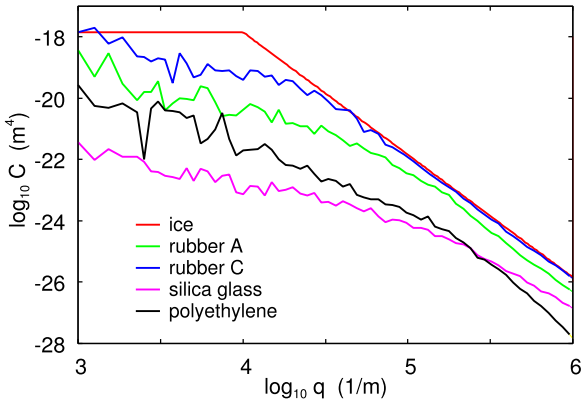


**FIG. 3.** Red line: The surface roughness power spectrum of the ice surface used in the viscoelastic friction calculations. The green, blue, black, and pink lines are the power spectra of the rubber compound A and C, and of the silica glass (SG) and polyethylene (PE) surfaces (after performing all the experiments), respectively. The glass surface is scratched, and this is the reason for its relative large power spectrum for large wavenumbers. The rms roughness values of the A, C, SG, and PE surfaces are 11.9, 11.7, 0.40, and 1.15 $\mu$m, respectively. The corresponding rms slopes are 0.42, 0.60, 0.24 and 0.20, respectively.

and C, and of the silica glass and polyethylene surfaces (after performing all the experiments), respectively. The glass surface was scratched, and this is the reason for its relative large power spectrum for large wavenumber. The two rubber surfaces are lapped (roughened) by sand paper to remove a skin layer. The rubber surface C is lapped for a longer time than the rubber surface A, but the larger roughness of the surface C may be due mainly to the pores (cavities) being exposed at the surface of this foam rubber compound.

In general, the surface roughness of the rubber, SG, and PE affects the area of real contact and the area of real contact contribution to the friction. However, during steady sliding at a constant speed over a smooth counter surface, there is no viscoelastic contribution to the friction from the rubber asperities as there is no time dependent deformation of the rubber.

## III. RUBBER–ICE FRICTION

### A. Rubber compound

In the present study, we use winter rubber tread compounds in the form of a solid block (compound A) and as a foam (compound C) with about 9% voids. The voids (spherical cavities) have diameters of the order $\lesssim 100\ \mu$m. The rubber compound consists of a mixture (blend) of equal amounts of natural rubber (NR) and butadiene rubber (BR), with carbon black filler. This is a winter tread compound with very low glass transition temperature ($T_g \approx -70\,^\circ$C for NR and $T_g \approx -100\,^\circ$C for BR). The dimension of the rubber block is 1 cm thick, 6 cm wide, and 2 cm long in the sliding direction.

The viscoelastic modulus of the rubber was measured using Dynamical Mechanical Analysis (DMA). We use a Q800 DMA instrument produced by TA Instruments. The machine is run in tension mode, meaning that a strip of rubber, clamped on both sides, is elongated in an oscillatory manner. The complex viscoelastic modulus $E(\omega)$ is first measured in constant strain mode with a strain amplitude of 0.04% strain and at different frequencies from 28 Hz stepwise down until 0.25 Hz (10 frequency points). The rather small strain amplitude is chosen in order to avoid/reduce strain softening effects, e.g., due to the Mullins effect or the Payne effect, which can strongly alter the viscoelastic response of the rubber specimen. Measuring the rubber sample in tension mode also requires to prestrain the rubber with a static strain that has to be larger than the dynamic strain during oscillation. A prestrain of 0.06% was applied in the experiments to avoid buckling the rubber during the DMA measurement.

The experiment starts at $-120\,^\circ$C, and after measuring the modulus in the frequency range mentioned earlier, the temperature is increased in steps of $5\,^\circ$C, and the procedure is repeated until $120\,^\circ$C is reached. The frequencies are then shifted in order to overlap in a smooth Re$E$ master curve. This temperature–frequency shifting procedure works strictly only for a compound consisting of one type of rubber with a well-defined glass transition temperature. In the present case, the compound consist of equal volume fractions of NR and BR and the shifting procedure can be considered only approximate.

In rubber sliding friction, the strain in the road asperity contact regions are typically rather high, ~0.1 – 1 (or ~10 – 100%). To take this into account, we "correct" the $E(\omega)$ master curve by performing strain sweeps out to strains of order ~1 (see, e.g., Ref. 39).

Figure 4 shows the logarithm of the real and imaginary part of the viscoelastic modulus $E(\omega)$ as a function of the logarithm of the frequency $\omega$. Figure 5 shows the logarithm of the shift factor $a_T$ as a function of the temperature, for the reference temperature $T_{\rm ref} = 20\,^\circ$C.

### B. Experimental results

We present experimental friction results for the nominal rubber–ice contact pressure $p_0 = 0.2$ MPa, as typical for tire applications. The temperature inside the deep-freezer is varied in steps from $-39\,^\circ$C to $\approx 0\,^\circ$C. We start at the lowest temperature, and for each

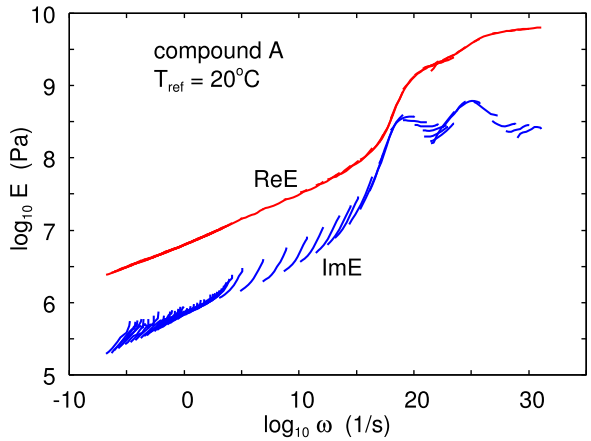


**FIG. 4.** The real and imaginary part of the viscoelastic modulus $E(\omega)$ as a function of the frequency $\omega$ (log–log scale) for compound A. If $\epsilon(t) = \mathrm{Re}[\epsilon(\omega)\exp(-i\omega t)]$ is the applied strain then the stress $\sigma(t) = \mathrm{Re}[E(\omega)\epsilon(\omega)\exp(-i\omega t)]$. For the reference temperature, $T = 20\,^\circ$C.

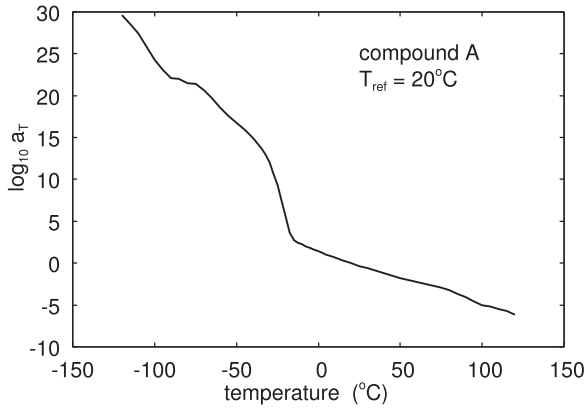


**FIG. 5.** The logarithm of the shift factor $a_T$ as a function of the temperature for compound A. For the reference temperature, $T = 20\,°C$.

temperature, the sliding speed is increased stepwise from 3 $\mu$m/s up to 1 cm $s^{-1}$. For the two lowest sliding speeds (3 and 10 $\mu$m/s), we slide 2 cm on the ice surface and for the six highest speeds (30, 100, 300 $\mu$m/s, 1, 3 and 10 mm $s^{-1}$) we slide 4 cm. So, the total sliding distance was 28 cm. The friction coefficients reported on below for each velocity are averages of $F_x/F_z$ over the sliding distance (2 or 4 cm). The experimental results presented in each figure below have been obtained on a fresh/virgin ice surface.

Additionally, the friction coefficients reported on below are averaged over forward and backward sliding, but the measured friction during forward and backward sliding are nearly identical in spite of the fact that the rubber block may be tilted in the sliding direction by a few degree relative to the ice surface.

Figure 6 shows the measured rubber–ice friction coefficient for compound A as a function of the logarithm of the sliding speed for several temperatures indicated. Similar results are shown for the foam compound C in Fig. 7. The rubber samples used in Figs. 6 and 7

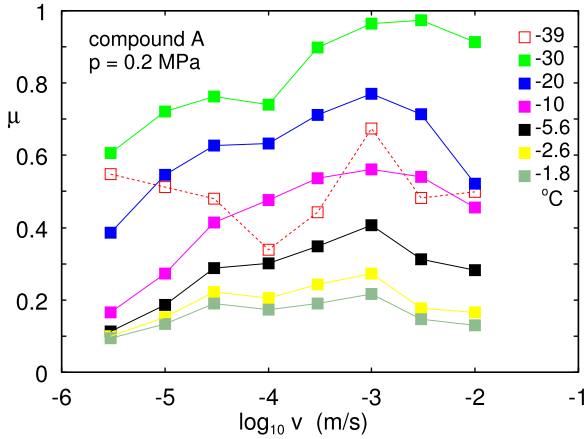


**FIG. 6.** Experimental rubber–ice friction coefficients for compound A as a function of the logarithm of the sliding speed for several temperatures indicated. The friction coefficient is averaged over the forward and backward sliding direction. The nominal contact pressure $p \approx 0.2$ MPa.

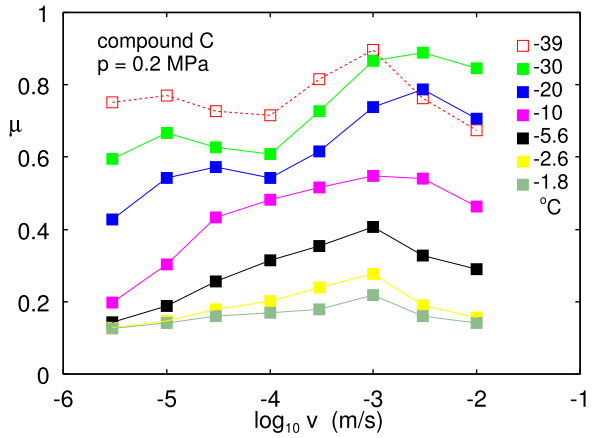


**FIG. 7.** Experimental rubber–ice friction coefficients for compound C as a function of the logarithm of the sliding speed for several temperatures indicated. The friction coefficient is averaged over the forward and backward sliding direction. The nominal contact pressure $p \approx 0.2$ MPa.

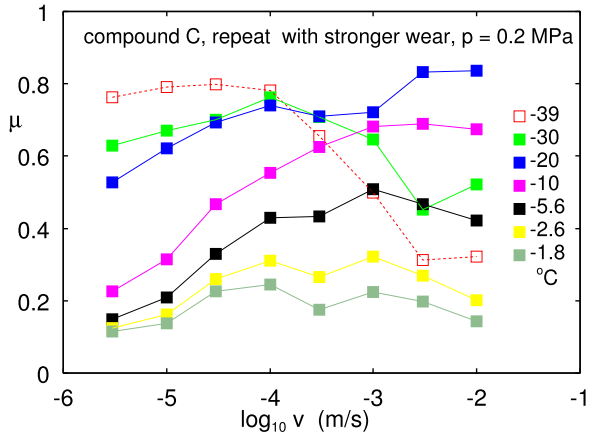


**FIG. 8.** Experimental rubber–ice friction coefficients for compound C (after surface lapped with sand paper) as a function of the logarithm of the sliding speed for several temperatures indicated. The friction coefficient is averaged over the forward and backward sliding direction. The nominal contact pressure $p \approx 0.2$ MPa.

were lapped by sand paper. For the foam compound, we performed a second experiment on a sample lapped for a longer time to remove enough rubber to make sure voids are exposed at the rubber surface, the result of which is shown in Fig. 8. Note the similarity in the measured friction in Figs. 6–8 in spite of the different ice surfaces used and of the different rubber surface preparation for the foam compound. Only the first run (open squares) at the lowest temperature $T = -39\,°C$ differs strongly comparing the three different experiments. We attribute this to run-in processes. As will be discussed later, ice wear processes occur when the sliding block is stiff and strongly affects the friction (see Figs. 14–16 below).

Figure 9 shows the measured rubber–ice friction coefficient for compound A as a function of the logarithm of the sliding speed

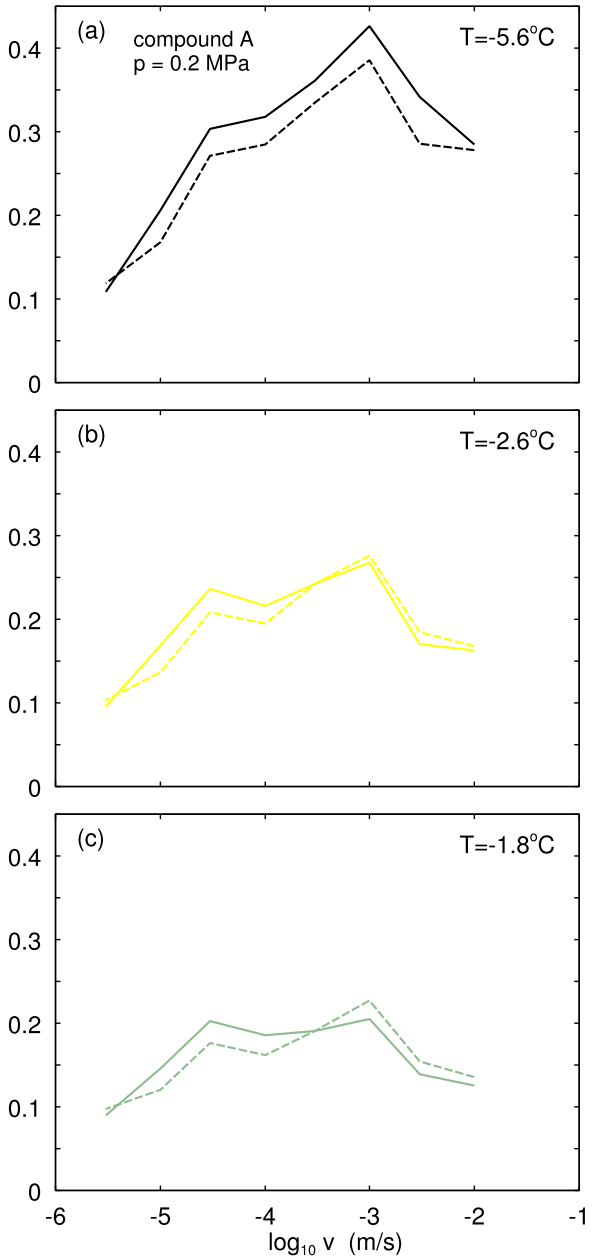


**FIG. 9.** Experimental rubber–ice friction coefficient for compounds A and C as a function of the logarithm of the sliding speed for the temperatures and $T = 0.5\,^{\circ}\mathrm{C}$ and $-1.1\,^{\circ}\mathrm{C}$ (compound C) and $T = -0.7$ and $0.2\,^{\circ}\mathrm{C}$ (compound A). The friction coefficient is averaged over the forward and backward sliding direction. The dotted lines are the repeat measurements on a new ice surface. The nominal contact pressure $p \approx 0.2$ MPa.

for several temperatures indicated. The solid line is for forward sliding, and the dashed line is for backward sliding motion. The friction coefficient is nearly the same in the two directions, which is not the case for elastically hard sliders, such as SG or PU sliders, unless the ice surface is very smooth (see Sec. IV).

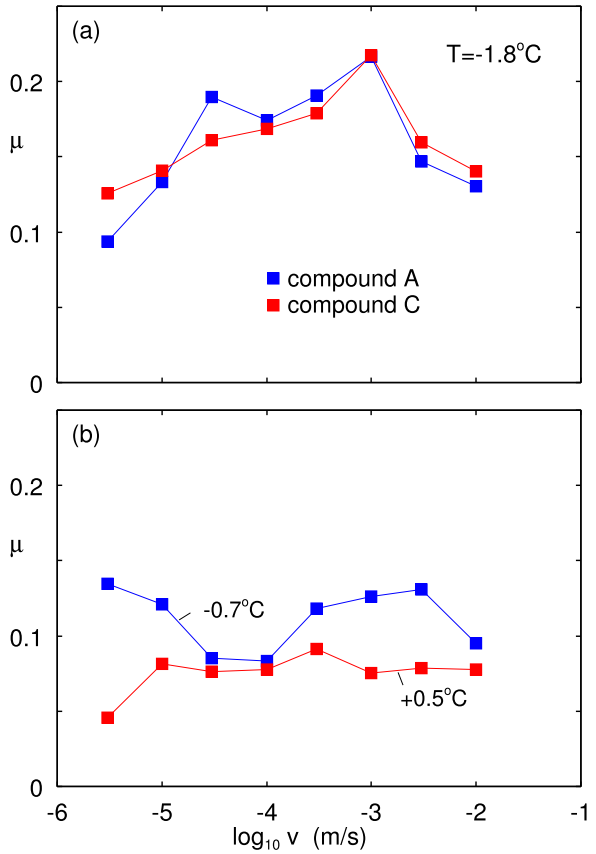


**FIG. 10.** Experimental rubber–ice friction coefficient for compound A (after surface weakly lapped with sand paper) as a function of the logarithm of the sliding speed for (a) $T = -5.6$, (b) $-2.6$, and (c) $-1.8\,^{\circ}\mathrm{C}$. The solid line is for forward sliding, and the dashed line is for backward sliding motion. The nominal contact pressure $p \approx 0.2$ MPa.

Experiments with tires indicate that tread blocks made by the foam compound show enhanced grip properties on wet ice at $T = 0\,^{\circ}\mathrm{C}$. To test this, we have performed friction experiments with compounds A and C on ice at $T \approx 0\,^{\circ}\mathrm{C}$ where a very thin melt-water film may exists on the ice surface. Figure 10 shows the measured rubber–ice friction coefficient for compound A and C as a function of the logarithm of the sliding speed for the temperature (a) $T = -1.8\,^{\circ}\mathrm{C}$ (from Figs. 6 and 7, respectively) and (b) $T = -0.7\,^{\circ}\mathrm{C}$ (compound A) and $+0.5\,^{\circ}\mathrm{C}$ (compound C). At least for the low sliding speeds, the friction for compound A is higher than for compound C, while on the dry ice surface at $T = -1.8\,^{\circ}\mathrm{C}$, the friction coefficients are very similar. However, the experiments are performed on different ice surfaces and slightly different temperatures, which could explain the rather small differences in the sliding friction values.

We performed another experiment close to the ice bulk melting temperature where compounds A and C were slid on the same ice surface after the surface had been run-in with compound A at a lower temperature. Figure 11 shows the measured rubber–ice friction coefficient as a function of the logarithm of the sliding speed for

temperatures $T = 0.5\,^{\circ}\mathrm{C}$ and $-1.1\,^{\circ}\mathrm{C}$ (compound C) and $T = -0.7$ and $0.2\,^{\circ}\mathrm{C}$ (compound A). The solid lines are taken from Fig. 10(b), while the dashed lines are the repeat measurements on a new ice surface.

### C. Analysis of experimental data and discussion

Two contributions to the rubber friction on ice are considered, namely, a contribution from shearing the area of real contact and a contribution from the viscoelastic deformation of the rubber surface by the ice asperities. In Refs. 1 and 34, we studied the viscoelastic contribution $\mu_{\mathrm{visc}}$ to the friction, and we will use the same theory in the present case. In the calculations, $\mu_{\mathrm{visc}}$ enters the viscoelastic modulus $E(\omega)$ of the rubber compound, as well as the ice surface roughness power spectrum $C(q)$ (see Ref. 40). We assume that the latter is similar to that of the ice surface I1 studied in Ref. 34; the power spectra used in the calculations below is given by the thick red line in Fig. 3. In Ref. 34, the large wavenumber cut-off $q_1$, which determines the shortest wavelength roughness included when calculating $\mu_{\mathrm{visc}}$, was determined so that the rubber–ice maximum contact stress is given by the plastic yield properties of the ice. However, in the present case, and also in Ref. 1, the roughness over all the length scales for which the power spectra were obtained in Ref. 34 ($q < 10^6\ \mathrm{m}^{-1}$) leads to contact stresses below the ice penetration hardness (which depends on the temperature and the indentation speed). In what follows, as in Ref. 1, we use $q_1 = 10^6\ \mathrm{m}^{-1}$ for all temperatures and sliding speeds. The exact origin and magnitude of the cut-off $q_1$ in the present case is not known to us, but using a larger wavenumber cut-off would result in a friction coefficient, which is larger than observed for the highest temperature.

Figure 12 shows the experimental rubber–ice friction coefficients for compound A as a function of the logarithm of the sliding speed for the temperatures $T = -1.8$, $-2.6$, and $-5.6\,^{\circ}\mathrm{C}$ (from Fig. 6). Also shown is the calculated viscoelastic contribution to the friction coefficient for compound A at $T = -1.8\,^{\circ}\mathrm{C}$, but the calculated contributions for $T = -2.6$ and $-5.6\,^{\circ}\mathrm{C}$ are nearly identical. In fact, the viscoelastic contribution to the friction is nearly the same even for very low temperatures, such as $T = -30\,^{\circ}\mathrm{C}$. This is due to the low glass transition temperature of the rubber compound.

Figure 13 shows the measured rubber–ice friction coefficient for compounds A and C as a function of the logarithm of the sliding speed for the temperature $T \approx 0\,^{\circ}\mathrm{C}$ [from Fig. 10(b)]. Also shown

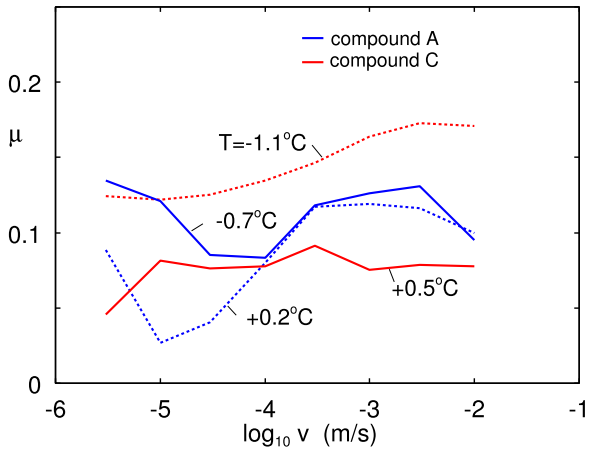


**FIG. 11.** Experimental rubber–ice friction coefficient for compounds A and C as a function of the logarithm of the sliding speed for the temperature (a) $T = -1.8\,^{\circ}\mathrm{C}$ (from Figs. 6 and 7, respectively) and (b) $T = 0.5\,^{\circ}\mathrm{C}$ (compound C) and $T = -0.7\,^{\circ}\mathrm{C}$ (compound A). The friction coefficient is averaged over the forward and backward sliding direction. The nominal contact pressure $p \approx 0.2$ MPa.

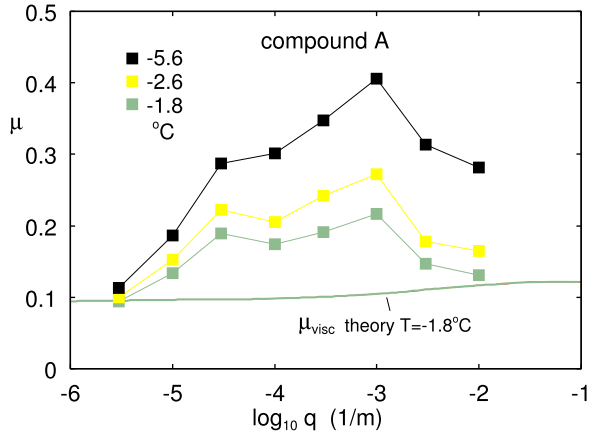


**FIG. 12.** Experimental rubber–ice friction coefficients for compound A as a function of the logarithm of the sliding speed for the temperature $T = -1.8$, $-2.6$, and $-5.6\,^{\circ}\mathrm{C}$ (from Fig. 6). Also shown is the calculated viscoelastic contribution to the friction coefficient for compound A at $T = -1.8\,^{\circ}\mathrm{C}$, but the calculated contributions for $T = -2.6$ and $-5.6\,^{\circ}\mathrm{C}$ are nearly identical.

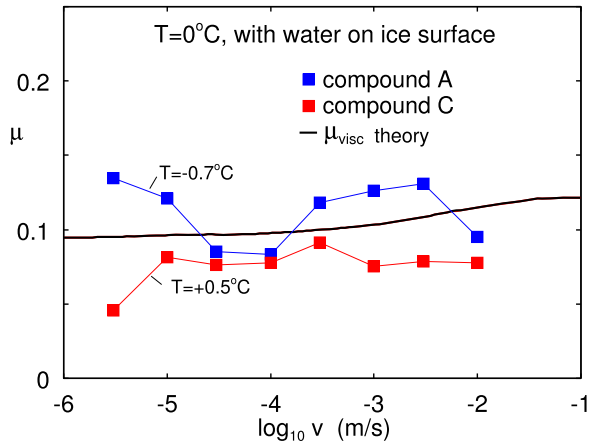


**FIG. 13.** Experimental rubber–ice friction coefficients for compounds A and C as a function of the logarithm of the sliding speed for the temperature $T \approx 0\,^{\circ}\mathrm{C}$ [from Fig. 10(b)]. Also shown is the calculated viscoelastic contribution to the friction coefficient for compound A at $T = 0\,^{\circ}\mathrm{C}$.

is the calculated viscoelastic contribution to the friction coefficient for compound A at $T = 0\,^{\circ}\mathrm{C}$. Since a very thin melt-water film may exist on the ice surface in this case, the roughness of the ice surface possibly differs from that of the ice at lower temperatures; ice melting may smooth the ice surface at least at small length scales. However, comparing the experimental data in Figs. 12 and 13, it does appear as if the friction continuously approaches the $T \approx 0\,^{\circ}\mathrm{C}$ curve as the temperature is increased toward the ice melting temperature. We conclude that, for temperatures close to the ice melting temperature, the friction force is likely mainly due to the rubber viscoelastic deformations by the ice asperities. The same conclusion was obtained in Refs. 1 and 34, but there we found that the viscoelastic contribution was dominating also for lower temperatures, at least down to $T = -5.4\,^{\circ}\mathrm{C}$. The rubber compounds used in Refs. 1 and 34 had a much higher $T_g$ (about $-45\,^{\circ}\mathrm{C}$) than for compound A used in this study, which resulted in a friction coefficient that increased strongly as the temperature was reduced below $T = 0\,^{\circ}\mathrm{C}$.

The viscoelastic contribution to the friction is expected to dominate if a thin pre-melted liquid-like water film occurs in the area

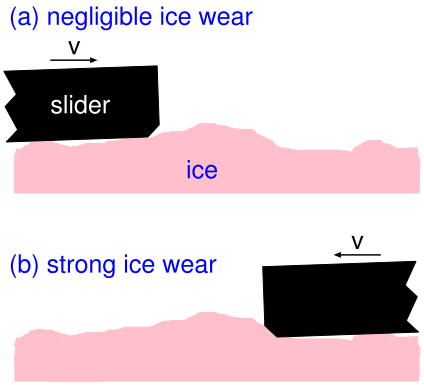


**FIG. 14.** The hard (PE or SG) slider scratches the ice surface. The resulting ice wear differs depending on the sliding direction due to a small tilting (of order of a few degree or less) of the slider relative to the ice surface and due to asymmetry (in the sliding direction) of the ice bumps. In the case illustrated, the friction will be strongly enhanced in the backward sliding direction when the slider hits into the ice bump. For rubber, the influence of the ice bump on the wear (and friction) is much smaller due to elastic deformations of the slider (the elastic modulus of the rubber in the rubbery region is lower than the plastic yield stress of the ice).

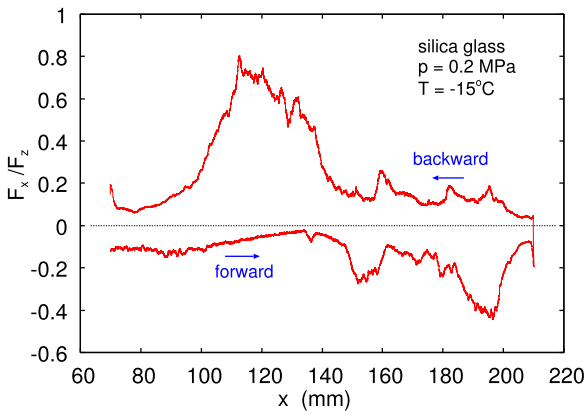


**FIG. 15.** Experimental SG–ice friction coefficients as a function of the position of the slider for $T = -15\,^{\circ}\mathrm{C}$ and sliding speed $v = 0.1\ \mathrm{mm\ s^{-1}}$. The nominal contact pressure $p \approx 0.2$ MPa.


**FIG. 16.** Ice surface after sliding in Fig. 15. Note the ice wear particles (white powder).

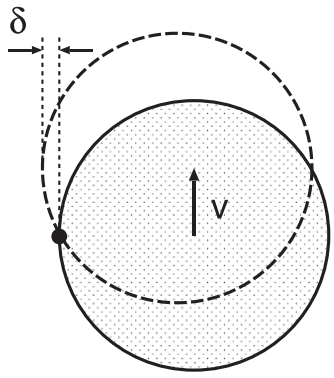


**FIG. 17.** A cylinder disk sliding on an ice surface with ice bumps. When the cylinder hits into a (high) bump, a locally enhanced friction force will act on the cylinder, and the cylinder will tend to pivot around the high-friction point, giving rise to a transverse displacement $\delta$ of the center of mass. The pivot point can occur with equal probability on the left and the right half of the cylinder, and a non-rotating cylinder will on the average move on a straight path. Imposing a rotation to the cylinder breaks the symmetry, and the cylinder moves to the left if the rotation in counterclockwise. The exact mechanism in which the rotation breaks the symmetry is not known.[46–48]

of real contact. At high (but not too high) sliding speeds, frictional heating becomes important, which may result in a pre-melted surface layer even at low temperature. At even higher sliding speeds, a melt-water film forms, which gives rise to a low friction, and in these cases, the viscoelastic contribution to the friction gains importance. However, for low temperature and low sliding speed, the measured friction is much larger than the viscoelastic contribution. This implies that there must be an important contribution from the area of real contact to the friction, and that no liquid-like film occurs in the rubber–ice contact regions in this case.

In Ref. 1 for another rubber compound with a higher glass transition temperature, it was shown that the measured rubber–ice friction coefficient is very similar to the measured ice–ice friction coefficient as a function of the sliding speed for $T < -10\,^{\circ}\mathrm{C}$. It was proposed that, for low temperatures, ice fragments attach to the rubber surface and that the slip occurs at the interface between the ice fragments and the ice surface. These ice fragments originate from ice wear processes during run-in (open squares in Figs. 6–8) or from frost crystals formed on the rubber and ice surfaces before sliding. We believe that ice fragments contribute to the rubber–ice friction in a similar way in the present case, but there must be an additional important contribution to the friction from the area of ice–rubber contact where in some contact regions slip occurs between the ice and the rubber. This is consistent with the experiments of Hemette *et al.*,[41] which we now discuss.

Hemette *et al.*[41] have performed rubber–ice friction studies for relative smooth ice surfaces for temperatures between $-20\,^{\circ}\mathrm{C}$ and $-2.5\,^{\circ}\mathrm{C}$. The nominal contact pressures they used are similar to those in our study, but they probably used much smoother ice surfaces. As a function of the logarithm of the sliding speed, they observed a Gaussian-like friction coefficient curve centered around $v \approx 10$ mm s$^{-1}$ with a maximum that decreased from ~2 at $-20\,^{\circ}\mathrm{C}$ to 0.2 at $-2.5\,^{\circ}\mathrm{C}$. For $T = -20\,^{\circ}\mathrm{C}$, this differs with Ref. 1 where the maximum of the friction at low temperature was observed for $v \approx 0.1$ mm s$^{-1}$ as also observed for the ice–ice contact. This discrepancy can be explained by assuming that, in the study of Hemette *et al.*, the sliding interface was devoid of frost crystals or ice wear particles and that slip occur between the rubber and the ice surface. In the present study, there appears to be two local maxima in the $\mu(v)$ curve at low temperature. This could result from some contact areas involving ice fragments sliding on the ice surface and other contact regions where the rubber slides on the ice surface.

The existence of a large rubber–ice frictional shear stress is supported by adhesion and friction experiments by Roberts and Richardson.[31,32] They found that rubber may adhere strongly to smooth (polished) ice surfaces (as strong as to silica glass) and that the friction coefficient between rubber and polished ice surfaces may be very large (of order 2) for low sliding speeds and low temperatures ($T < -10\,^{\circ}\mathrm{C}$, but $T > T_g$, where $T_g$ is the rubber glass transition temperature).[31,32]

At temperatures $T > -10\,^{\circ}\mathrm{C}$, the magnitude and the velocity dependency completely differ for the ice–ice contact compared to the ice–rubber contact. For the ice–ice contact, the friction decreases drastically with increasing sliding speed $v$, while this is not the case for the rubber–ice contact. For the ice–ice contact, we have shown in Ref. 42 that the drop in the friction with increasing $v$ can be explained by pre-melting of the ice surface as a result of frictional heating. However, at a low sliding speed, frictional heating is negligible, and in this case, even at $T = -3\,^{\circ}\mathrm{C}$, there is no pre-melted liquid-like film at the ice–ice interface and the ice–ice sliding friction coefficient is very large,[43] while for rubber on ice the friction is much lower. For $T > -10\,^{\circ}\mathrm{C}$, we propose that the rubber–ice friction is due to the viscoelastic contribution, and a contribution from shearing the area of real contact that may involve a pre-melted film with non-Newtonian properties as found in recent molecular dynamics calculations.[18]

## IV. SILICA GLASS (SG)–ICE FRICTION

When the slider is made of an elastically hard material, such as PE or SG, we observe strong wear of the ice surface unless it is very smooth. This effect is illustrated in Fig. 14, which shows schematically a slider on an ice surface with a bump. The slider scratches the ice surface, but the resulting ice wear depends on the sliding direction due to a small tilting (of order a few degree or less) of the slider relative to the ice surface and due to some asymmetry (in the sliding direction) of the ice bump. In the case illustrated, the friction will be strongly enhanced in the backward sliding direction when the slider hits into the ice bump. For rubber, the influence of ice bumps on the wear (and friction) is much smaller due to elastic deformations of the slider (the elastic modulus of the rubber in the rubbery region is lower than the plastic yield stress of the ice), except at very low temperatures where the rubber is in its glassy state. For this reason, we observe very small changes in the friction for a rubber slider when the sliding direction is reversed (see Fig. 11). To reduce the wear of the ice surface, we have cut off the edges of the rectangular SG, PE, and rubber blocks at 45° angle, as indicated in Fig. 14.

For PE or SG, unless the ice surface is very smooth, we observe large fluctuations in the friction with the position $x$ on the sliding track and the sliding direction. This is illustrated in Fig. 15,

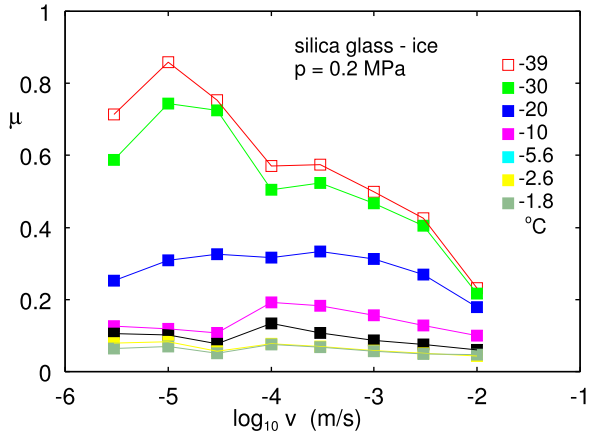


**FIG. 18.** Experimental SG–ice friction coefficient as a function of the logarithm of the sliding speed for several temperatures indicated on a new very smooth ice surface. The friction coefficient is averaged over the forward and backward sliding direction. The nominal contact pressure $p \approx 0.2$ MPa.

which shows the measured SG–ice friction coefficient as a function of the position of the slider for $T = -15\,^{\circ}\mathrm{C}$ and the sliding speed $v = 0.1$ mm s$^{-1}$. Figure 16 shows the ice surface after sliding in Fig. 15. Note the ice wear particles (white powder).

We have found that strong wear and high friction obviously occur when the sliding block hits into bumps on the ice surface. However, if the bumps would all have equal heights and could be densely enough distributed, the sliding friction would be reduced at least at high sliding speeds where a thin melt-water film would have formed. This effect is well known in curling.[44–48]

In curling, fine water droplets are sprayed onto the flat ice surface. These droplets freeze into small bumps or "pebbles," which are "shaved" to form flat upper surfaces of nearly equal height. The curling stones, which have curved surfaces (i.e., have no sharp edges), "ride" on the pebbles as they slide down the ice. The pebbles reduce friction and enable the stones to travel farther than if the ice is not pebbled. The reason for this is that the pebbles concentrate the weight of the stone (about 200 N) onto a smaller ice area than if there was only flat (pebble-less) ice. The resulting frictional heating can melt the thin surface layers of the pebbles, resulting in very small friction coefficients, typically $\mu \approx 0.01$ at sliding speeds of order ~1 m/s.

In curling, the granite cylinder is initially given both a rotation (angular momentum) and a forward momentum. On a perfectly smooth ice surface, the cylinder would move on a straight path in spite of the imposed rotation. Thus, pebbling is essential as without it a curling stone would not curl. Curling stones sliding on scraped ice surfaces, which show roughness with large fluctuations in the heights of the bumps, exhibit even larger curl distances than with a surface covered by pebbles.[49] The curl is most likely related to the large increase in the friction observed above when a sliding block hits into an ice bump: the pebbles are not all of exactly equal height and the curling block will experience a rapidly fluctuating (in time and space) friction force that will make the curling stone curl. This can be understood in the limiting case where the friction becomes infinitely large in one small area. In this case, the curling block will rotate around the pinning point as indicated in Fig. 18. This could move the curling block either to the right or the left (depending on the position of the pinning point), but a small initial rotation of the block will break the symmetry (exactly how is not known) and the block will move in the direction of rotation.[46–48] It is remarkable that the curl distance is nearly independent of the rotation speed initially imposed on the curling stone.

To obtain results for SG (and PE) not dominated by the ice wear process illustrated earlier, it is necessary to use very smooth ice surfaces. However, even in these cases, we cannot exclude some influence by ice wear processes. In Fig. 17, we show the measured silica glass–ice friction coefficient on a very smooth ice surface, as a function of the logarithm of the sliding speed for several temperatures indicated in the figure. The friction coefficient is again averaged over the forward and backward sliding directions. Note that for the temperatures $T = -39\,^{\circ}\mathrm{C}$ and $T = -30\,^{\circ}\mathrm{C}$, the friction coefficient is very large (~0.3 – 0.8 depending on the sliding speed), but for $T \approx -2\,^{\circ}\mathrm{C}$, it is only ~0.05 and only weakly velocity dependent.

Silica glass is hydrophilic, and after cleaning with isopropanol, in normal atmosphere it will quickly be covered by a thin film consisting of water and some organic contamination. When cooled to low enough temperature, this film may freeze forming a thin ice-like film (with organic contamination) on the glass surface. Thus, the silica glass–ice system may exhibit a sliding friction of similar magnitude as for the ice–ice interface. For the two lowest temperatures ($T = -38\,^{\circ}\mathrm{C}$ and $T = -30\,^{\circ}\mathrm{C}$), this is indeed the case, but for $T > -10\,^{\circ}\mathrm{C}$, for sliding speeds <1 mm s$^{-1}$, the friction for the ice–glass interface is much smaller than for the ice–ice interface.

Experiments have shown that a pre-melted water film exists at the interface between silica and ice for $T > -20\,^{\circ}\mathrm{C}$ (see Ref. 22). In one experiment, where an ice slab was produced by freezing water in contact with a silica surface (i.e., the ice is in full contact with the silica surface), a lateral force resulted in ice block sliding (adhesive failure) on a silica surface for $T > -20\,^{\circ}\mathrm{C}$, while cohesive failure occurs for $T < -25\,^{\circ}\mathrm{C}$. However, sliding (adhesive failure) was only observed on very smooth silica surfaces ($R_a < 0.4$ nm), while cohesive failure was observed for all temperatures $T < 0\,^{\circ}\mathrm{C}$ on a silica surface with bigger roughness ($R_a \sim 6$ nm). In Ref. 23, one of us has explained the different behavior as due to ice–silica adhesion and the elastic energy stored at the interface when sliding the ice block away from its initial position.

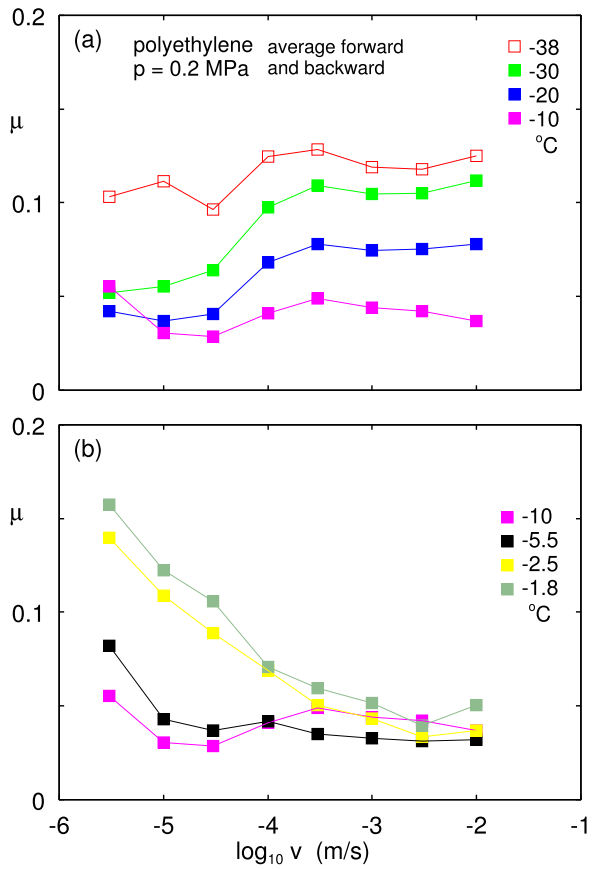


**FIG. 19.** Experimental polyethylene–ice friction coefficients as a function of the logarithm of the sliding speed for (a) $T \leq -10\,^{\circ}\mathrm{C}$ and (b) $T \geq -10\,^{\circ}\mathrm{C}$ on a very smooth ice surface. The friction coefficient is averaged over the forward and backward sliding direction. The nominal contact pressure $p \approx 0.2$ MPa.

## V. POLYETHYLENE (PE)–ICE FRICTION

As for SG, unless the ice surface is very smooth, for polyethylene (PE), we observe similarly strong fluctuations in the friction force with the position $x$ along the ice track. This is again caused by the slider hitting ice bumps, resulting in a plowing-type of PE–ice interactions and to the formation of ice wear particles. To avoid (or reduce) this, we prepared ice surfaces as smooth as possible.

Figure 19 shows the measured polyethylene–ice friction coefficients as a function of the logarithm of the sliding speed for several temperatures on such a very smooth ice surface. The friction coefficient is averaged over the forward and backward sliding direction. There appears to be a qualitative difference in the frictional behavior for temperatures above and below $-10\,^{\circ}$C. Thus, for $T < -10\,^{\circ}$C, the friction increases slightly with increasing sliding velocity, while for $T > -10\,^{\circ}$C, the opposite occurs. For $T < -10\,^{\circ}$C, the friction coefficient is much smaller than observed for silica glass and the rubber slider. For temperatures between $-10$ and $-2\,^{\circ}$C and sliding speeds ~1 cm s$^{-1}$, the PE and silica glass exhibit very similar friction coefficients of order ~0.04.

Figure 19 shows that the ice–PE interface exhibits low friction for all temperatures and sliding speeds studied. It is remarkable that, for temperatures close to the ice melting temperature ($T = -2.6\,^{\circ}$C and $-1.8\,^{\circ}$C), the friction coefficient increases with decreasing sliding speed for $v < 0.1$ mm s$^{-1}$. This could be attributed to a creep-enhancement of the contact area, but then one would expect it to occur also for the ice–SG interface, which is not the case. However, the friction also depends on the shear stress acting on the area of real contact that could have different velocity dependencies for the SG–ice and PE–ice interfaces.

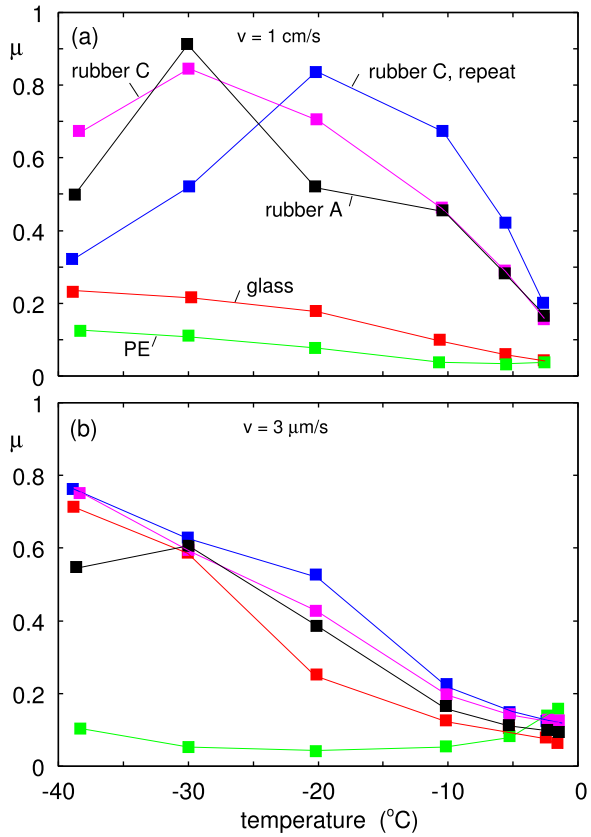


**FIG. 20.** The measured friction for the ice–rubber, ice–PE, and ice–SG systems as a function of the temperature for (a) the velocity $v = 1$ cm s$^{-1}$ and (b) $v = 3\ \mu$m/s. The friction coefficient is averaged over the forward and backward sliding direction. The nominal contact pressure $p \approx 0.2$ MPa.

## VI. DISCUSSION

In the study above, we have discussed the dependency of the sliding friction coefficient on the sliding speed for many temperatures. Here, we plot the same numerical data as a function of the temperature for the highest and the lowest sliding speed considered earlier.

Figure 20 shows the measured friction for the ice–rubber, ice–PE, and ice–SG systems as a function of the temperature for (a) the velocity $v = 1$ cm s$^{-1}$ and (b) $v = 3\ \mu$m/s. In all cases, except PE, the friction decreases on approaching the ice bulk melting temperature. We interpret this as due to increased thickness and mobility of the water molecules of the pre-melted liquid-like film expected at the interface when the ice temperature approaches the ice bulk melting temperature. For PE at the lowest sliding speed $v = 3\ \mu$m/s, the friction coefficient increases on approaching the ice bulk melting temperature.

Polyethylene is used for winter sport equipment, e.g., for skis. The small sliding speeds considered above may be relevant for uphill movement in skiing with PE skis, where no or negligible slip is wanted, but most experimental studies have focused on much higher sliding speeds where frictional heating produces a melt-water film.

Detailed studies of the friction between polyethylene and ice have been presented by Bäurle *et al.*[6,7] and Stamboulides.[8] These studies are for different conditions than in our study, but are consistent with our results. Thus, in Fig. 21, we show the measured PE–ice friction coefficient from Fig. 19(b) (squares) and Ref. 8 (stars). The measurements are performed at very different nominal contact pressures (0.2 and 0.005 MPa, respectively) and slightly different temperatures (the dashed lines connect data obtained for similar temperatures), but the two datasets can be joined smoothly by interpolation (dashed lines).

Two recent studies have proposed very different origins of the friction on ice. Reference 50 showed the importance of the plowing contribution, while in Ref. 51, it was found that during reciprocated sliding on ice a lubricating, viscous mixture of liquid water and ice particles dominates the frictional behavior. For PE and SG sliders, we have also observed a plowing-like contribution to the friction where the rectangular blocks wear the ice surface bumps resulting in ice fragments (white powder). At higher sliding speeds where melt-water is also produced, the ice wear particles may be suspended in liquid water giving rise to an ice slurry that could act as a lubricant during reciprocated sliding as found in Ref. 51. This is similar to the ice slurry that sometimes occurs on roads in winter and generates low friction and dangerous driving conditions, as one of us has experienced.

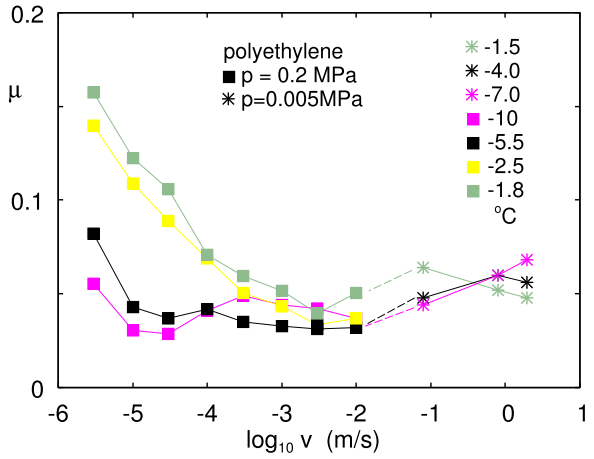


**FIG. 21.** The measured PE–ice friction coefficient from Fig. 19(b) (squares) and Ref. 8 (stars). The measurements are performed at very different nominal contact pressures (0.2 and 0.005 MPa, respectively) and slightly different temperatures (the dashed lines connect data obtained for similar temperatures).

Another recent study addressed high-speed ice skating. In Ref. 52, it was shown that the friction between the steel skate blade and the ice stems from boundary friction where the temperature of the interface is below zero and ice surface molecules exhibit unconventional mobility and hydrodynamic friction where the ice melts and a thin water layer between the blade and the ice forms. The boundary friction only plays a role at the tip of the skate blade over an extremely short contact length between the skate blade and the ice and gives a negligible contribution to the total friction but dissipates enough heat to melt the ice allowing the skater to slide smoothly on a thin layer of melt water.

In general, for sliding speeds above $\approx 0.1 - 1$ m/s, the frictional heating is high enough to melt a thin ice layer and the friction is determined mainly by fluid dynamics at an interface with a complex gap (surface separation) determined by the surface roughness. In this paper, we have focused on low sliding speeds $v \leq 1$ cm s$^{-1}$ where the ice does not melt but where ice pre-melting may result in a thin liquid-like film that strongly reduces the sliding friction force. We note that the nature of the friction force for low sliding speeds is very important for tire dynamics as it determines the effective static friction force and hence the line separating the region where the tread blocks do not slide (or slide at very low speed, say $v < 1$ mm s$^{-1}$) from the region where sliding appears (typical slip velocity ~1 m/s).

Experience have shown that at low sliding speeds the friction between a ski and snow (ice particles) increases with increasing magnitude of the ski base surface roughness, while at high sliding speeds it decreases.[53] The former effect may be due to plowing of the ice particles by the ski surface asperities. Section IV (see also Ref. 50) shows that the plowing contribution to the friction can be very large. At high sliding speeds, a thin melt-water film occur in the ice–ski contact regions and the plowing contribution to the friction will be smaller, in particular, if the water film thickness becomes comparable to the amplitude of the surface roughness at the length scale where plowing would occur for the dry contact (note: the system may deform elastically at large length scales). In this case, increasing surface roughness may result in a smaller capillary suction effect (the contribution to the normal force from capillary adhesion depends on the surface area covered by water and the water film thickness). Having a hydrophobic surface of the ski (as is the case for wax coated skies and uncoated skies made from polyethylene) will also reduce the capillary suction effect (by increasing the water contact angle) as discussed in Ref. 1.

## VII. SUMMARY AND CONCLUSION

We have studied the velocity and temperature dependency of the friction force when the rectangular blocks of compact rubber, foam rubber, silica glass (SG), and polyethylene (PE) are slid on ice surfaces. The most important results are as follows:

(1) The compact rubber and the foam rubber exhibit very similar frictional properties in the studied velocity ($3\ \mu$m/s $< v < 1$ cm s$^{-1}$) and temperature ($-40\,^{\circ}$C $< T < 0\,^{\circ}$C) interval.
(2) The viscoelastic contribution dominates the rubber friction on ice close to the ice bulk melting temperature.
(3) For rubber–ice friction, for low temperatures, an important contribution to the friction comes from ice fragments attached to the rubber surface resulting in ice–ice friction,[1] but an additional contribution is derived from the adhesive rubber–ice interaction in contact regions where no ice fragments are attached to the rubber.[9,41]
(4) For SG and PE, the friction on ice is very sensitive to ice bumps that result in ice wear and to a very high friction when the sliding block hits into the bumps. This is a type of plowing contribution to the wear and friction. The same effect is not observed for rubber blocks that can deform elastically and move on top of the bump with small wear and small change in the friction force.
(5) PE exhibits low friction ($\mu < 0.15$) for all studied temperatures and sliding speeds, while SG exhibits friction coefficients of order 1 at low temperatures ($T < -30\,^{\circ}$C) and low sliding speeds.
(6) For rubber and SG sliders, the friction forces decreases as the temperature approaches the ice bulk melting temperature, which we attribute to the increased mobility of the water molecules and the increased thickness of the pre-melted film. For rubber and SG sliders, this effect dominates over the increased contact area expected as the ice penetration hardness decreases with increasing temperature. For the PE slider, the friction coefficient instead increases as the temperature approaches the ice bulk melting temperature, in particular, at the lowest sliding speed, possibly due to a different velocity dependency of the shear stress in the area of real contact compared to rubber and SG.
(7) For sliding speeds 1 cm $> v >$ 1 mm s$^{-1}$ and temperatures $T > -6\,^{\circ}$C, the SG and PE blocks give similar almost velocity-independent friction coefficients $\mu \sim 0.04$, while the rubber friction coefficients are larger (between 0.3 and 0.1) and decreasing with increasing temperature.
(8) For PE blocks, the measured friction coefficients for temperatures $T > -7\,^{\circ}$C are consistent with measurements

performed by other groups at higher sliding speeds (up to 2 m/s).

## AUTHOR DECLARATIONS

### Conflict of Interest

The authors have no conflicts to disclose.

### Author Contributions

**N. Miyashita**: Conceptualization (equal); Investigation (equal). **A. E. Yakini**: Investigation (equal). **W. Pyckhout-Hintzen**: Investigation (equal). **B. N. J. Persson**: Conceptualization (lead); Investigation (lead); Software (lead); Writing – original draft (lead).

## DATA AVAILABILITY

The data that support the findings of this study are available from the corresponding author upon reasonable request.

## APPENDIX: ICE ADHESION TO GLASS SURFACES

People living in countries with cold winters know that it is not easy to remove ice formed on automobile windshields. Window glass, e.g., windshields, are produced from float glass. Float glass is a sheet of glass made by floating molten glass on a bed of molten metal, typically tin. This results in very smooth surfaces, which, in ideal cases, would have surface roughness resulting only from frozen capillary waves. Frozen capillary waves have the surface roughness power spectrum (see, e.g., Ref. 54)

$$C(q) = \frac{1}{(2\pi)^2}\frac{k_b T^*}{\rho g + \gamma q^2}. \tag{A1}$$

Here, we have assumed that when reaching the temperature $T^*$ the diffusive movement of the atoms in the glass becomes so slow that the capillary waves that exist at this temperature are frozen. Note that the gravity term $\rho g$ becomes important only for very small wavenumber roughness, namely, for $q < (\rho g/\gamma)^{1/2} \approx 300\ \mathrm{m}^{-1}$, and the gravity term can be neglected in most cases giving $C(q) \sim q^{-2}$, which corresponds to a self-affine fractal surface with the Hurst exponent $H = 0$ (and fractal dimension $D_f = 3$). For such surfaces, the rms slope is determined mainly by the shortest (nanometer) wavelength roughness.

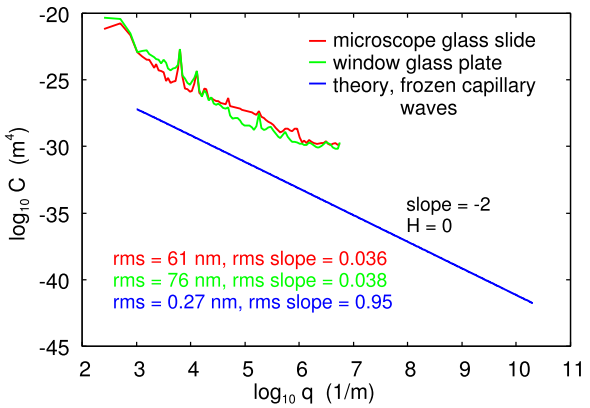


**FIG. 22.** The theoretical surface roughness power spectrum of a glass surface due to frozen capillary waves (blue lines) and the measured power spectrum of a microscope glass slide (red line) and for a window glass surface (green line).

The blue line in Fig. 22 shows the theoretical power spectrum given by (A1) with $T^* = 600$ K, $\gamma = 0.3\ \mathrm{J/m^2}$ and $\rho = 2200\ \mathrm{kg/m^2}$. Including the roughness wavenumber range $q_0 < q < q_1$ indicated in the figure ($q_0 = 300\ \mathrm{m}^{-1}$ and $q_1 = 2 \times 10^{10}\ \mathrm{m}^{-1}$) gives the rms roughness amplitude $h_{\mathrm{rms}} = 0.27$ nm and the rms slope $\xi = 0.95$. Theory[23] shows that because of the large rms slope for frozen capillary waves, displacing ice frozen onto a glass surface result in cohesive failure rather than adhesive failure. (The theory shows that the elastic energy per unit surface area produced when the ice displaced away laterally from its original position is $U_{\mathrm{el}}/A_0 \approx 0.45\ \mathrm{J/m^2}$.) This explains why it is hard to remove ice from the windshields of cars even for temperatures (say $T = -5$ C) where one expects a very thin water film of pre-melted ice.

The long wavelength roughness on glass surfaces may be much larger than predicted by the capillary wave theory due to effects such as the influence of mechanical vibrations during the cooling from the liquid state, or weathering. To illustrate this, we show in Fig. 22 the measured (small wavenumber) power spectra of a microscope glass slide (red line) and a widow glass plate (green line), both of which was kept for several years uncovered in the normal atmosphere. The power spectra was calculated from the topography measured using an engineering stylus instrument (Mitutoyo Portable Surface Roughness Measurement Surftest SJ-410 with a diamond tip with the radius of curvature $R = 1\ \mu$m). We used the tip–substrate repulsive force $F_N = 0.75$ mN, the scan length $L = 25$ mm, and the tip speed $v = 50\ \mu$m/s. The glass surfaces was cleaned using isopropanol. Including only the wavenumber regions indicated in the figure, the glass surfaces have the rms roughness 61 and 76 nm, but the rms slopes are only 0.036 and 0.038 in spite of the fact that the power spectra are $\sim 10^4$ times bigger (corresponding to ~100 times bigger roughness amplitude) than for the ideal theory prediction (blue line). This demonstrates that the rms slope for surfaces with the Hurst exponent $H = 0$ is determined by the nanoscale roughness. Since the rms-slope in practical cases cannot be much larger than 1 (see Ref. 55), it also implies that at a short length scale the roughness on the two studied glass surfaces are likely to be similar to the theory prediction (blue line). Thus, the power spectra given by the red and green lines in Fig. 22 must bend down toward the blue line for larger wavenumbers.

## REFERENCES

[1] T. Tada, S. Kawasaki, R. Shimizu, and B. N. J. Persson, "Rubber–ice friction," Friction 1–10 (2023).
[2] R. Rosenberg, "Why is ice slippery?," Phys. Today **58**(12), 50 (2005).
[3] A.-M. Kietzig, S. G. Hatzikiriakos, and P. Englezos, "Physics of ice friction," J. Appl. Phys. **107**, 081101 (2010).
[4] J. F. Nye, "Glacier sliding without cavitation in a linear viscous approximation," Proc. R. Soc. A **315**, 381 (1970).
[5] B. N. J. Persson, "Ice friction: Glacier sliding on hard randomly rough bed surface," J. Chem. Phys. **149**, 234701 (2018).

[6]L. Bäurle, T. U. Kaempfer, D. Szabó, and N. D. Spencer, "Sliding friction of polyethylene on snow and ice: Contact area and modeling," Cold Reg. Sci. Technol. **47**, 276 (2007).
[7]L. Bäurle, D. Szabó, M. Fauve, H. Rhyner, and N. D. Spencer, "Sliding friction of polyethylene on ice: Tribometer measurements," Tribol. Lett. **24**, 77 (2006).
[8]C. Stamboulides, "Microscopic ice friction of polymeric substrates," Ph.D. thesis, The University of British Columbia, Vancouver, 2010.
[9]S. Hemette, "Rubber-ice friction: A multi-scale and multi-physical approach," Ph.D. thesis, University of Lyon, 2019.
[10]N. Orndorf, S. Singla, and A. Dhinojwala, "Transition in the acid-base component of surface free energy of ice upon the premelting of its second molecular bilayer," J. Phys. Chem. C **124**, 19588 (2020).
[11]M. Faraday, "On regelation, and on the conservation of force," Philos. Mag. **17**, 162 (1859).
[12]M. Demmenie, P. Kolpakov, Y. Nagata, S. Woutersen, and D. Bonn, "Scratch-healing behavior of ice by local sublimation and condensation," J. Phys. Chem. C **126**, 2179 (2022).
[13]J. W. M. Frenken and J. F. v. d. Veen, "Observation of surface melting," Phys. Rev. Lett. **54**, 134 (1985).
[14]B. Slater and A. Michaelides, "Surface premelting of water ice," Nat. Rev. Chem. **3**, 172 (2019).
[15]R. Lipowsky, "Critical surface phenomena at first-order bulk transitions," Phys. Rev. Lett. **49**, 1575 (1982).
[16]U. Tartaglino, T. Zykova-Timan, F. Ercolessi, and E. Tosatti, "Melting and nonmelting of solid surfaces and nanosystems," Phys. Rep. **411**, 291 (2005).
[17]L. Baran, W. Rzysko, P. Llombart,and L. G. MacDowell, "Ice friction at the nanoscale," PNAS **119**, e2209545119 (2022).
[18]Y. Zhao, Y. Wu, L. Bao, F. Zhou, and W. Liu, "A new mechanism of the interfacial water film dominating low ice friction," J. Chem. Phys. **157**, 234703 (2022).
[19]J. G. Dash H. Fu and J. S. Wettlaufer Rep. Prog. Phys. **58**, 115 (1995).
[20]Y. Qiu and V. Molinero, "Why is it so difficult to identify the onset of ice premelting?," J. Phys. Chem. Lett. **9**, 5179 (2018).
[21]Y. Li and G. A. Somorjai, "Surface premelting of ice," J. Phys. Chem. **111**, 9631 (2007).
[22]J. F. D. Liljeblad, I. Furo, and E. C. Tyrode, "The premolten layer of ice next to a hydrophilic solid surface: Correlating adhesion with molecular properties," Phys. Chem. Chem. Phys. **19**, 305 (2017).
[23]B. N. J. Persson, "Ice breakloose friction," J. Chem. Phys. (submitted).
[24]W. D. Bascom, R. L. Cottington, and C. R. Singleterry, "Ice adhesion to hydrophilic and hydrophobic surfaces," J. Adhes. **1**, 246 (1969).
[25]J. Thomson, "On recent theories and experiments regarding ice at or near its melting-point," Proc. R. Soc. London **10**, 151 (1860).
[26]F. P. Bowden and T. P. Hughes, "The mechanism of sliding on ice and snow," Proc. R. Soc. London, Ser. A **172**, 280 (1939).
[27]F. P. Bowden, "Friction on snow and ice," Proc. R. Soc. Lond. A **217**, 462 (1953).
[28]K. A. Emelyanenko, A. M. Emelyanenko, and L. B. Boinovich, "Water and ice adhesion to solid surfaces: Common and specific, the impact of temperature and surface wettability," Coatings **10**, 648 (2020).
[29]E. S. Thomson, H. Hansen-Goos, J. S. Wettlaufer, and L. A. Wilen, "Grain boundary melting in ice," J. Chem. Phys. **138**, 124707 (2013).
[30]M. Torabi Rad, G. Boussinot, and M. Apel, "Dynamics of grain boundary premelting," Sci. Rep. **10**, 21074 (2020).
[31]A. D. Roberts, "Rubber-ice adhesion and friction," J. Adhes. **13**, 77 (1981).
[32]A. D. Roberts and J. C. Richardson, "Interface study of rubber-ice friction," Wear **67**, 55 (1981).
[33]D. D. Higgins, B. A. Marmo, C. E. Jeffree, V. Koutsos, and J. R. Blackford, "Morphology of ice wear from rubber-ice friction tests and its dependence on temperature and sliding velocity," Wear **265**, 634 (2008).
[34]O. Lahayne, B. Pichler, R. Reihsner, J. Eberhardsteiner, J. Suh, D. Kim, S. Nam, H. Paek, B. Lorenz, B. N. J. Persson, and J. Persson, "Rubber Friction on Ice: Rubber friction on ice: Experiments and modeling," Tribol. Lett. **62**, 17 (2016).
[35]A. J. Tuononen, A. Kriston, and B. Persson, "Multiscale physics of rubber-ice friction," J. Chem. Phys. **145**, 114703 (2016).
[36]C. Klapproth, T. M. Kessel, K. Wiese, and B. Wies, "An advanced viscous model for rubber–ice–friction," Tribol. Int. **99**, 169 (2016).
[37]A. Almqvist, B. Pellegrini, N. Lintzén, N. Emami, H.-C. Holmberg, and R. Larsson, "A scientific perspective on reducing ski-snow friction to improve performance in Olympic cross-country skiing, the biathlon and Nordic combined," Front. Sports Act. Living **4**, 844883 (2022).
[38]K. Kalliorinne, J. Sandberg, G. Hindér, R. Larsson, H.-C. Holmberg, and A. Almqvist, "Characterisation of the contact between cross-country skis and snow: A macro-scale investigation of the apparent contact," Lubricants **10**, 279 (2022).
[39]T. V. Tolpekina and B. N. J. Persson, "Adhesion and friction for three tire tread compounds," Lubricants **7**, 20 (2019).
[40]B. N. J. Persson, "Theory of rubber friction and contact mechanics," J. Chem. Phys. **115**, 3840 (2001).
[41]S. Hemette, J. Cayer-Barrioz, and D. Mazuyer, "Thermal effects versus viscoelasticity in ice-rubber friction mechanisms," Tribol. Int. **162**, 107129 (2021).
[42]B. N. J. Persson, "Ice friction: Role of non-uniform frictional heating and ice premelting," Chem. Phys. **143**, 224701 (2015).
[43]F. E. Kennedy, E. M. Schulson, and D. E. Jones, "The friction of ice on ice at low sliding velocities," Philos. Mag. A **80**, 1093 (2000).
[44]M. Denny, "Ice deformation explains curling stone trajectories," Tribol. Lett. **70**, 41 (2022).
[45]M. Denny, "A first-principle model of curling stone dynamics," Tribol. Lett. **70**, 84 (2022).
[46]M. R. A. Shegelski and E. P. Lozowski, "Pivot–slide model of the motion of a curling rock," Can. J. Phys. **94**(12), 1305 (2016).
[47]H. Nyberg, S. Alfredson, S. Hogmark, and S. Jacobson, "The asymmetrical friction mechanism that puts the curl in the curling stone," Wear **301**, 583 (2013).
[48]J. Murata, "Study of curling mechanism by precision kinematic measurements of curling stone's motion," Sci. Rep. **12**, 15047 (2022).
[49]E. T. Jensen and M. R. Shegelski, "The motion of curling rocks: Experimental investigation and semi-phenomenological description," Can. J. Phys. **82**, 791 (2004).
[50]R. W. Liefferink, F.-C. Hsia, B. Weber, and D. Bonn, "Friction on ice: How temperature, pressure, and speed control the slipperiness of ice," Phys. Rev. X **11**, 011025 (2021).
[51]L. Canale, J. Comtet, A. Nigues, C. Cohen, C. Clanet, A. Siria, and L. Bocquet, "Nanorheology of interfacial water during ice gliding," Phys. Rev. X **9**, 041025 (2019).
[52]M. E. H. van Dongen and D. M. J. Smeulders, "Ice speed skating: Onset of lubrication by frictional heating," Europhys. Lett. **134**, 34005 (2021).
[53]K. Kalliorinne, B. N. J. Persson, J. Sandberg, G. Hinder, R. Larsson, H.-C. Holmberg and A. Almqvist, "Characterisation of the contact between cross-country skis and snow: A micro-scale study considering the ski-base texture," Lubricants (submitted).
[54]B. N. J. Persson, "Contact mechanics for randomly rough surfaces," Surf. Sci. Rep. **61**, 201 (2006).
[55]B. N. J. Persson, "On the fractal dimension of rough surfaces," Tribol. Lett. **54**, 99 (2014).